

# A Lightweight Convolution and Vision Transformer integrated model with Multi-scale Self-attention Mechanism<sup>★</sup>

Yi Zhang<sup>a</sup>, Lingxiao Wei<sup>a</sup>, Bowei Zhang<sup>a</sup>, Ziwei Liu<sup>b</sup>, Kai Yi<sup>c,\*</sup> and Shu Hu<sup>a</sup>

<sup>a</sup>Department of Computer Science, Sichuan University, China

<sup>b</sup>School of Computer Science, Nanyang Technological University, Singapore

<sup>c</sup>Sichuan Police College, Intelligent Policing Key Laboratory of Sichuan Province, Luzhou, China

## ARTICLE INFO

### Keywords:

Vision Transformer (ViT)  
Convolutional Neural Networks (CNNs)  
Multi-scale self-attention  
Lightweight architecture

## ABSTRACT

Vision Transformer (ViT) has prevailed in computer vision tasks due to its strong long-range dependency modelling ability. However, its large model size with high computational cost and weak local feature modeling ability hinder its application in real scenarios. To balance computation efficiency and performance, we propose SAEViT (Sparse-Attention-Efficient-ViT), a lightweight ViT based model with convolution blocks, in this paper to achieve efficient downstream vision tasks. Specifically, SAEViT introduces a Sparsely Aggregated Attention (SAA) module that performs adaptive sparse sampling based on image redundancy and recovers the feature map via deconvolution operation, which significantly reduces the computational complexity of attention operations. In addition, a Channel-Interactive Feed-Forward Network (CIFFN) layer is developed to enhance inter-channel information exchange through feature decomposition and redistribution, mitigating redundancy in traditional feed-forward networks (FFN). Finally, a hierarchical pyramid structure with embedded depth-wise separable convolutional blocks (DWSCConv) is devised to further strengthen convolutional features. Extensive experiments on mainstream datasets show that SAEViT achieves Top-1 accuracies of 76.3% and 79.6% on the ImageNet-1K classification task with only 0.8 GFLOPs and 1.3 GFLOPs, respectively, demonstrating a lightweight solution for various fundamental vision tasks.

## 1. Introduction

ViT has achieved remarkable results in various vision tasks (e.g. classification[31], detection[12] and segmentation[15] etc.) due to its powerful global modeling capabilities. To integrate convolution neural network (CNN) with prior knowledge and local feature extraction capability into ViT, existing methods[6] have explored several fusion schemes with great success. MetaFormer[35] proved that the architecture of ViT is beneficial for improving the performance. To enhance model accuracy, some works[25] tried to refine the original attention computation by introducing multi-scale self-attention mechanisms (e.g. integrating features of different resolutions during attention operation). However, they usually add 2–4 additional multi-scale computation modules, which causes significant computational overhead and also impedes their applications in real-time scenarios. To mitigate computation cost, traditional methods employed multi-level hierarchical architectures that down-sample feature maps progressively or adopted sliding window strategies in spatial dimension. However, they relied on a fixed sliding window, which can easily ignore the correlation of local information. Other methods[32] performed sub-sampling on keys (K) and values (V) in attention computation to further reduce the computation cost.

On the other hand, the classical feed-forward network (FFN) in ViT typically consists of fully connected layers

for channel-wise computation, which lacks explicit inter-channel modeling ability. While some works[33] attempted to enhance the expressivity of FFN by appending convolutional blocks or DWSCConv to improve local feature modeling, which still overlooked inter-channel interactions.

To address the above mentioned challenges and design an advanced backbone for vision tasks, we propose a simple yet effective Transformer block that combines local perception and long-range modeling on the basis of multi-level pyramid structure. Firstly, we integrate convolutional feature processing modules into the model to incorporate convolutional prior knowledge. Then, we adopt a sparse attention approach for feature extraction to reduce the computational cost of attention operation. By leveraging the redundancy of similar pixels in the input image, the aggregation of local features and sparse sampling are performed to ensure long-range dependencies of attention. To mitigate potential accuracy loss by sparse attention and enhance inter-channel interactions, we replace FFN layer by CIFFN, which decomposes feature channels and reassign feature weights explicitly to preserve representational capacity under lightweight constraints.

Built upon the above design principle, we propose SAEViT, a lightweight model that combines the strengths of CNNs and ViT. SAEViT originates from convolution+Transformer hybrid structure and sparse attention, while we focus on lightweight design for edge devices by striking a balance between performance and efficiency. Specifically, SAEViT's sparse attention module achieves faster computation than Spatial Reduction Attention (SRA) and Window-based Attention, without introducing additional computational overhead. We evaluate model performance primarily through accuracy and throughput. Throughput measures

\* This research was funded by the Intelligent Policing Key Laboratory of Sichuan Province, No.ZNJW2024KFMS004.

\*Corresponding author.

E-mail address: yikai@scpolicec.edu.cn (K. Yi).

inference efficiency, reflecting the real-time applicability and computational resource utilization. Higher throughput indicates more images/data samples processed per second. We develop 2 model variants with different computational complexities: Tiny (T) and Extra Small (XS), but both have  $\leq 10\text{M}$  parameters and  $\leq 1.5\text{GFLOPs}$ . We compare our model with other lightweight models in this paper, and our model indeed has less parameters and lower computation cost than other competing methods, which is supposed to be deployed under resource restricted situations. Experiments include image classification, object detection, and semantic segmentation. On ImageNet, SAEViT-t achieves 76.3% Top-1 accuracy with 0.8 GFLOPs, while the SAEViT-xs variant reaches 79.6% with 1.3 GFLOPs. Comparison of throughput will be reported in Section 4.4.

In a nutshell, the main contributions of this work include:

- A unified ViT framework has been proposed, which integrates CNNs and ViT to acquire the feature prior capabilities of CNN as well as the long-range dependency modeling ability of attention mechanisms.
- The traditional aggregation attention mechanism has been redesigned to address the high computational cost. Compared to traditional window attention and SRA, SAEViT achieves significantly higher throughput.
- A channel-interactive Feed-Forward Network has been developed to counteract potential accuracy degradation caused by sparse attention. Meanwhile, channel interaction has been performed to improve the expressivity of FNN the training accuracy under lightweight constraints.

## 2. Related Works

### 2.1. Vision Transformer

The rise of attention mechanisms promoted the popularity of ViT in the field of computer vision. As a result, a series of excellent works have emerged [18, 29, 7], which significantly improves the performances of ViT based models (in terms of efficiency and accuracy). To enhance the overall feature extraction and generalization capabilities of models, many works focus on optimizing ViT's computational paradigm, particularly through the fusion of convolution blocks and attention mechanisms. Extensive experiments demonstrate that integrating CNN with ViT is an effective way for feature extraction and improving performance gain. Other approaches [38, 32, 18] aim to improve feature utilization efficiency by facilitating cross-layer feature interactions.

Recently, huge efforts have been made in reducing the spatial dimensions of Multi-Head Self-Attention (MHSA) module, which is normally a computational bottleneck in ViT architectures. MHSA maps input tensors into key, query and value tensors. Recent studies revealed that key and value tensors can be subsampled with minimal accuracy loss, achieving a better efficiency-accuracy trade-off. For instance, MaxViT[29] employed blocked local attention

and dilated global attention to perform global and local spatial interactions across arbitrary inputs. Biformer[41] introduced a novel bi-level routing attention mechanism, enabling flexible computational allocation and content-aware dynamic sparse attention for improved efficiency and performance. Clusterformer[14] utilized clustering mechanism that is integrated within Transformer architecture to realize a universal vision model. ProMotion[20] is a Transformer based motion model that calculates optical flow and estimates scene depth. Considering the original intention of lightweight design, we perform sparse attention operation on the feature maps rather than sub-sampling keys and values.

### 2.2. The Feed-Forward Network

The FFN layer is a critical component in ViT. Its primary role is to introduce non-linear transformations and enhance the model's representational capacity. By expanding and compressing channel dimensions in high-dimensional spaces, it enriches the feature representation of individual tokens within the architecture. It not only affects the model's expressiveness but also ViT's computational efficiency and practical deployment. Consequently, ensuing works attempted to enhance FFN layers through convolutional operations to strengthen local features (e.g. PVTv2[33], SRFormer[40], LightViT[10]). Others, from architectural perspective, modified the residual connections by designing inverted residual blocks to enhance cross-layer gradient propagation (e.g. CMT[6]). Partially inspired by the above works, we focus on designing learnable parameters of FFN that interact with input feature maps to dynamically redistribute channel-wise parameters. Combining with SAA, our approach effectively boosts feature extraction capabilities while maintaining computational efficiency.

### 2.3. Lightweight ViT

Considering that ViT suffers high computational cost, which hinders its application in resource constrained scenarios. Designing lightweight ViT is a research area of great significance. Current lightweight ViT designs mainly focus on latency reduction on real devices, optimizing GPU and CPU throughputs, and reducing the computational overhead of attention mechanisms and overall architecture. RepViT[30] replaced the Transformer's multi-head self attention (MSA) module with lightweight convolutional blocks. It adopted a multi-branch structure during training to enrich feature representations, and merged these branches into an efficient convolutional layer for inference. Meanwhile, it adjusted the number of channels and network depth to reduce parameters, which turns out to realize effectively lower on device latency. MobileViT[21] employed a hybrid architecture with unfold-transform-fold operations, achieving higher accuracy while reducing FLOPs. EfficientViT[1] effectively boosted both accuracy and GPU throughput by revising the inverted bottleneck structure and introducing cascaded group attention.

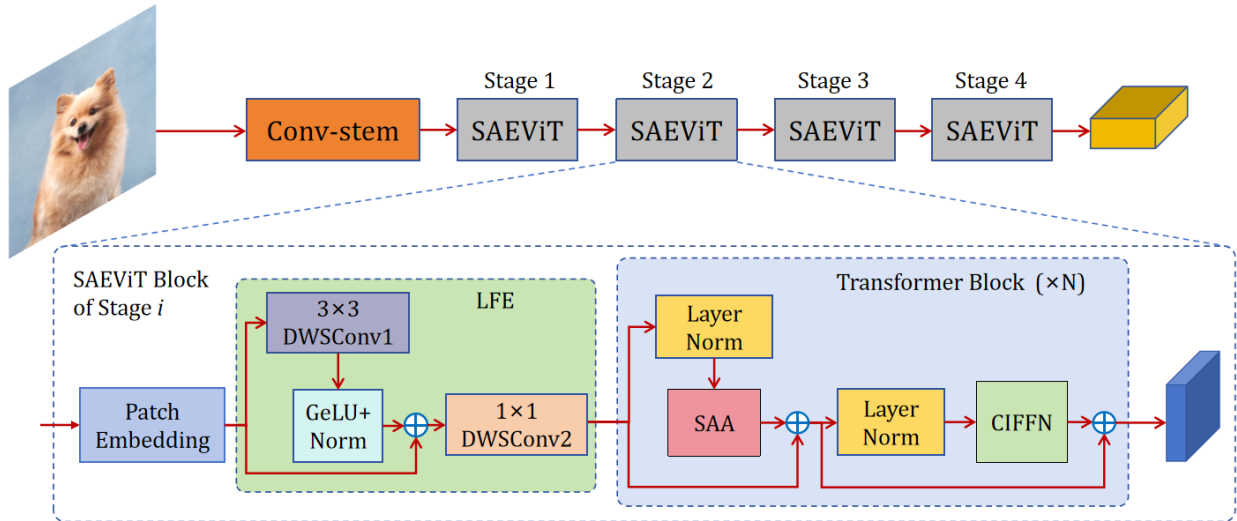


**Fig. 1:** The overall architecture of the proposed SAEViT. The input is first processed by convolutional stems followed by 4 stages of SAEViT blocks, each of which applies Patch Embedding followed by Local Feature Extraction (LFE) and stacked Transformer modules with Sparsely Aggregated Attention (SAA) and Channel-Interactive FFN (CIFFN).

### 3. Method

Our goal is to combine the strength of convolutional neural networks (CNN) with the attention mechanisms, and develop a lightweight ViT based architecture. Following the design principle of pyramid network, our model is divided into 4 stages, each of which produces feature maps of different scales to capture multi-scale image information for detection and segmentation tasks. Between each stage, Patch Embedding layers (which consists of convolution and normalization operations) are adopted to down-sample the resolution to half of its original value. In Section 4.5.4, the convolution stems are proved to be effective at boosting accuracies in multiple downstream vision tasks. Accordingly, our convolution stem is built upon 2 convolution layers (with kernel size=3, stride=1, padding=1). Meanwhile, we stack various Transformer blocks at each pyramid layer to meet diverse task requirements and computational resource constraints. Each Transformer blocks share the same internal structure, which is comprised of a SAA module and a CIFFN. The overall architecture of our proposed model is shown in Fig. 1.

To construct a hybrid convolution-ViT structure, we connect Local Feature Extraction (LFE)[36] module with modified Transformer block. LFE is an embedding layer with DWSCov and an activation function, which refines the input features to the Transformer block. Inside the Transformer block, SAA module rectifies the sampling strategy by performing the sparse block-wise sampling on the feature map in an adaptive way, which reduces the computational load of traditional attention mechanisms. To deal with information redundancy and limited feature expressivity in high-dimensional features, we rectify FNN by employing inter-channel interaction mechanism. To be specific, a  $1 \times 1$

convolution is firstly applied to map the input features into a higher dimensional space. Then, depth-wise convolution (DWConv) is used to enhance features within each channel, enriching the feature content. An activation function is then introduced to introduce non-linearity, further improving the model's fitting ability. During channel interaction, a customized decomposition layer and an element-wise scaling layer are used to redistribute and adjust features across channels, enhancing inter-channel information exchange. Finally, another  $1 \times 1$  convolution maps the features back to their original dimension. Our approach significantly reduces information redundancy and enhances the model's capability to represent complex features.

The extracted features are sent to a global average pooling layer to yield global feature representation, which is then followed by a classification layer with a softmax function that ultimately produce the final classification results. Based on this, SAEViT effectively addresses the inefficient feature processing mechanism in traditional ViT, which also provides an efficient and lightweight solution for vision tasks.

#### 3.1. Sparsely Aggregated Attention

**The core idea of SAA originates from the fact that in vision-related tasks, adjacent image patches often have high redundancies (i.e. they share high similarities).** To mitigate the redundancy and also to capture long-range spatial dependencies, we replace the standard attention block with SAA in our lightweight model, so that the model will be able to filter out and integrate tokens that carry similar information (i.e. reduce the number of tokens and computation costs). **SAA is featured by spatial sampling strategy: by down-sampling the tokens with a rate  $s_r$ , so that only the features in the key regions are retained. To be specific, the stride**

of down-sampling is set to  $sr$  to aggregate the adjacent tokens with high similarity. Then, each non-overlapping  $sr \times sr$  window is reduced to 1 token through average pooling. It not only reduces the complexity of attention operation, but also preserves the main information within the window through local feature smoothing, avoiding the loss of key details caused by random sampling. This is similar to MaxViT[23]'s "Sparse Global Attention" and Biformer[33]'s "Dynamic Sparse Routing" approach, both of them reduce computational complexity through spatial down-sampling. However, unlike them, SAA later up-samples the feature map via deconvolution so as to recover the original spatial dimension. Deconvolution takes a small sized input feature map and outputs a larger feature map, which restores the spatial structural information through a learnable convolution kernel (i.e. enlarging the size by inserting zeros between input elements and performing standard convolution). For given sizes of input feature maps, if the stride is set to  $s$ , then the intermediate expended feature map could be created by inserting  $s-1$  number of zeros between each row and column of each spatial unit. Then, a learnable convolution kernel with a size of  $k \times k$  is used to convolve the feature map and the output size is controlled by boundary padding.

Compared to traditional methods (e.g. bilinear interpolation), the main advantage of deconvolution is that it parameterizes the up-sampling process and makes it learnable. The convolution kernel is not fixed, instead, it is dynamically optimized through back propagation in model training. As a result, deconvolution learns and reconstructs spatial feature patterns that are highly relevant to specific tasks in an adaptive way. Meanwhile, deconvolution also inherits the key characteristics of standard convolution operation: Local connectivity and weight sharing. This means that each output pixel is only generated by weighted combinations of elements within the corresponding local neighborhood in the input feature map, and the weights of the same set of convolution kernels slide across the entire input space for reuse. Because of this, deconvolution has a context-aware feature reconstruction ability. This ability not only increases the spatial dimension of feature maps, but also restores important details based on the local context of input data.

SAA is comprised of a reversible sparsity mechanism that is quite different from traditional fixed window or uniform sampling methods. The calculation flow is shown in Fig. 2.

Assume the input feature map to the attention block at each stage is written as  $X_{in} \in R^{H \times W \times C}$ , where  $H$ ,  $W$ , and  $C$  represent the height, width, and number of channels, respectively. The spatial down-sampling rate is set to  $sr$  (i.e. a token could be aggregated for every  $sr \times sr$  windows). Let the aggregation operation be denoted as Aggregation Down-sampling (ADS):

$$ADS(X) = AvePooling_{sr \times sr}(X_{in}) \quad (1)$$

$$X_1 = ADS(Norm(X_{in})) \quad (2)$$

Here, *AvePooling* refers to an average pooling operation determined by the down-sampling rate at each layer of the

network backbone, which balances the performances and computation overhead. The down-sampling rate aims to balance the computational complexity and model performance and is controlled by pre-defined model parameters. When  $sr > 1$ , a down-sampling operation will be performed on the input feature map. Although it reduces computational load, it inevitably causes information loss. We thereby set a reasonable stride of the pooling operation so as to control the down-sampling size. The sparsely down-sampled Q, K, and V are then further processed through the attention module as follows:

$$X_2 = Attn(X_1) \quad (3)$$

Here *Attn* represents the conventional attention computation.

The parameter plays a critical role in both down-sampling and subsequent up-sampling operations. When  $sr > 1$ , after self-attention computation, a deconvolution layer is employed to up-sample the feature map, restoring it to its original spatial dimensions. The deconvolution layer is configured with a kernel size =  $sr$  and stride =  $sr$ , ensuring that the up-sampled feature map matches the size of the original input feature map. Let  $L_{LocalProp}$  denote the deconvolution layer with kernel size and stride equal to  $sr$ . In deconvolution operation, the input feature maps are divided into  $C$  groups according to the channel dimension. Then the final output  $X_{out}$  is generated via:

$$X_{out} = L_{LocalProp}(X_2) + X_{in} \quad X \in R^{C \times H \times W} \quad (4)$$

$$L_{LocalProp} = Deconv(kernel\_size = sr, stride = sr) \quad (5)$$

Based on this, the computation cost of attention operation can be effectively reduced to 1/4 of the original, thereby enhancing the computation efficiency. Further analysis will be provided in Section 4.4.2 comparing the number of parameters, the computation costs and CPU/GPU throughput among several classical attention blocks.

### 3.2. Channel Interaction Feedforward Network Layer

A standard FFN is typically composed of fully connected layers. However, redundancy exists across different channels when dealing with high-dimensional features. In addition, the linear transformation in fully connected layers applies the same operation to all channels, lacking effective screening mechanism and integration of inter-channel information. As a result, the model may overly focus on some unimportant information during training while ignoring the correlations between channels, compromising the model's expressive power and generalization abilities. To address this issue, most existing methods directly implant channel enhancement modules, such as the Squeeze-and-Excitation (SE) module, into the FFN. Meanwhile, the non-linear transformations in conventional FFN often apply activation functions to the outputs of fully connected layers, which may only capture insufficient multi-scale and hierarchical features under complex feature distributions. Under such circumstances, we

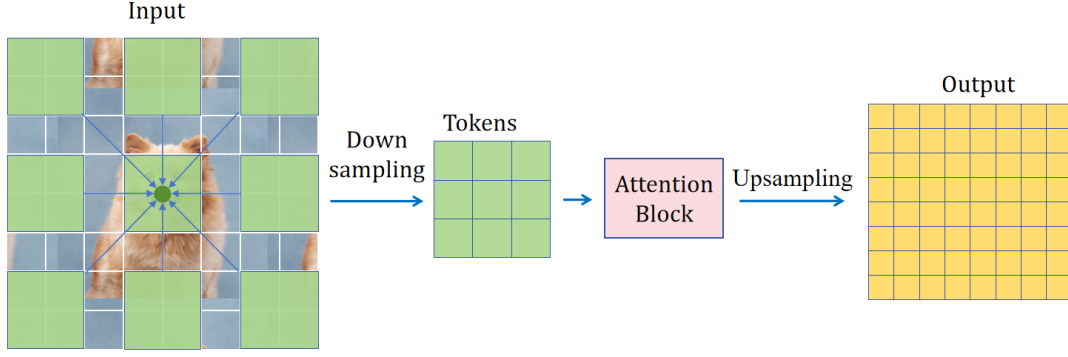


**Fig. 2:** The Feature Scaling Process of SAA. The input is first down-sampled to retain only informative tokens based on redundancy, which is then processed by attention block. Finally, it is up-sampled via deconvolution to reconstruct the full-resolution output.

propose CIFFN, which consists of convolutional layers for channel mapping, DWConv for local information extraction, and a feature decomposition module for decomposing and recombining features. A comparison has been made among FFN, depth-wise separable (DWS) FFN and CIFFN in Fig. 3. The computation flow of CIFFN is expressed as:

$$FD(X) = y_c \times (X + Conv(X)) + X \quad (6)$$

$$CIFFN(X) = Conv_2(FD(Conv_1(X)) + X) \quad (7)$$

where FD refers to feature decomposition module.  $y_c$  is a learnable channel-wise scaling factor which is initialized to 0. The convolution operation (Conv), is used for feature compression, reducing the number of channels in the input. Given the input feature map, the computation flow of CIFFN is expressed as:

$$X_1 = GELU(DWConv(Conv_1(Norm(X_{in}))) \quad (8)$$

$$X_2 = FD(X_1) \quad (9)$$

$$X_{out} = Conv_2(X_2) + X_{in} \quad (10)$$

It employs a  $3 \times 3$  DWConv to process the features. Subsequently, a  $1 \times 1$  convolution layer, referred to as  $Conv_1$ , is utilized to compress the input channels, effectively reducing the dimensionality of the feature map. Following this, another  $1 \times 1$  convolution layer ( $Conv_2$ ) is applied to restore the channel dimensions to their original size.

Our CIFFN effectively addresses the incompatibility problem by unifying local perception and context aggregation capabilities. It leverages parallel DWConv to capture interactions across different FFN layers, which captures more interaction information from the intermediate-layers and generates discriminative multi-order representations with minimum computational cost. Furthermore, it mitigates inter-channel information redundancy, enhancing channel efficiency and the model's representational capacity. It also redistributes the channel features in an adaptive way through the lightweight design. Compared to standard FFNs and DWS FFNs, CIFFN achieves superior performance with lower computation cost.

### 3.3. The configuration of the proposed SAE Block

In this section, we will discuss the structural details of SAEViT-XS and SAEViT-T. For the  $i$ -th stage, assume the output channel dimension is  $C$ , "head" denotes the number of heads, "n" refers to the number of blocks. Suppose "sr" is the down-sampling rate for SAA. Then the model structure could be expressed by Table 1. We select sr based on the characteristics of the feature maps retained in each layer. The parameters should be suitable for the size of the network and feature maps, which also balance information preservation and computational overhead. In the shallow stage (with  $56 \times 56$  resolution), a larger sampling rate (such as  $sr=8$ ) is used to actively reduce redundant tokens, while in the deep stage (such as  $7 \times 7$ ),  $sr=1$  is used to preserve detailed features. As described in Section 3.1, these stride sizes are preset to achieve a reasonable balance between accuracy and FLOPs (within 1.5G).

The Conv-stem is responsible for data preprocessing. To construct a Conv-stem, we use a combination of convolution operations. Firstly, we use a  $3 \times 3$  convolution for down-sampling, which not only reduces the spatial dimension of the data, but also extracts basic features from the image. Next, we use 2 convolution blocks with kernel size of 3, stride of 1, and padding of 1. These 2 convolution blocks further refine and enrich features through layer-wise convolution, so that the processed data has high-quality feature expression, which is then sent to the next SAE.

## 4. Experiments

In this section, multiple visual recognition experiments have been conducted to verify the effectiveness of our proposed model. First, our model is pre-trained on ImageNet-1K[4] for image classification task, which is compared with other popular in terms of accuracy and computational cost. Besides, the performances for object detection and segmentation are also tested on COCO [17] and ADE20K[39] respectively. The processing speeds for feature maps are analyzed and compared with other competitors.

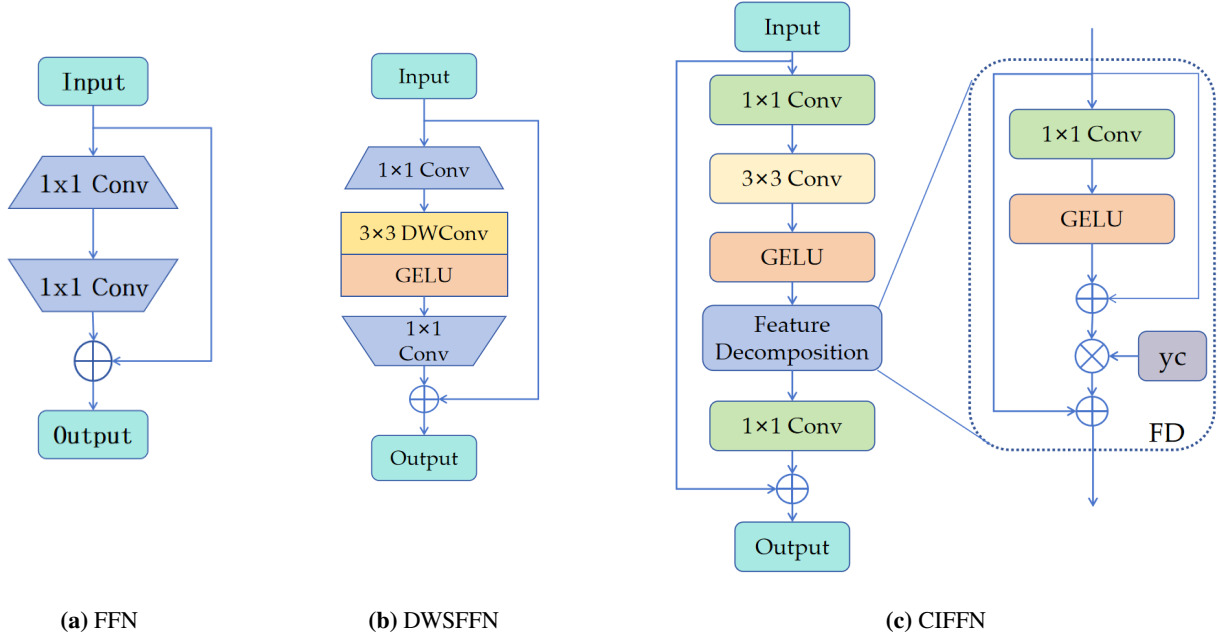


Fig. 3: Comparison of structures among FFN, the depth-wise separable FFN, and CIFFN.

Table 1

The structure of the proposed SAE Block.

	Output size	Layer Name	SAEViT-T	SAEViT-XS
Stage1	112*112	Conv-stem	C=24	C=24
Stage2	56*56	SAEBlock	C=48, head=2, sr=8, n=1	C=48, head=2, sr=8, n=1
Stage3	28*28	SAEBlock	C=96, head=4, sr=4, n=1	C=96, head=4, sr=4, n=2
Stage4	14*14	SAEBlock	C=192, head=8, sr=2, n=3	C=192, head=8, sr=2, n=5
Stage5	7*7	SAEBlock	C=384, head=16, sr=1, n=2	C=384, head=16, sr=1, n=3

#### 4.1. Image Classification

ImageNet-1K contains approximately 1.28M training images and 50K validation images across 1K categories, which cover a wide variety of objects and scenes, providing sufficient and diverse data resources for model training and evaluation. Following DeiT[28], we utilize AdamW optimizer for fine-tuning, and set the batch size to 256, weight decay coefficient to  $5 \times 10^{-2}$  and set momentum to 0.9. The model is trained 300 epochs with an initial learning rate of  $1 \times 10^{-3}$ , and a linear warm up strategy is applied during the first 5 epochs. After warm up, the learning rate will be adjusted following a cosine decay schedule. Data augmentation techniques are adopted, including random cropping, random horizontal flipping, random erasing, and label smoothing. During training, images are randomly cropped to  $224 \times 224$  pixels. All experiments are conducted on 2xNVIDIA 3090 GPUs.

**Results:** A comparison of classification results are made between our model and other popular methods, including MobileNetV2[26] and EfficientNet[27] as well as PVT[32], PVTv2[33], and DeiT[28]. All methods are roughly divided into 2 groups based on their number of parameters and floating-point operations (FLOPs). As shown in Table 2,

under comparable network size, SAEViT achieves higher accuracy than other peers.

#### 4.2. Object Detection and Instance Segmentation

Object detection has been conducted on COCO dataset, where the training set contains 118k images and the validation set contains 5k images. We utilize 2 commonly used detectors (RetinaNet[16] and Mask R-CNN[8]) to validate the effectiveness of SAEViT as a backbone network.

Before training, the model initializes the SAEViT backbone with pre-trained weights from the ImageNet dataset and applies Xavier initialization to the newly added layers. Our model is trained on 2 RTX 3090 GPUs, with a batch size of 8 and AdamW optimizer, where the initial learning rate is set to  $1 \times 10^{-4}$ . Following common practices, the model is fine-tuned with 1x schedule (i.e. 12 epochs). The shorter side of input images is resized to 800 pixels, while the longer side does not exceed 1333 pixels. For testing, the shorter side of input images is fixed at 800 pixels.

For RetinaNet,  $AP_{50}$  refers to the mean Average Precision (mAP) with an Intersection over Union (IoU) threshold of 0.5, and  $AP_{75}$  corresponds to mAP with an IoU threshold of 0.75.  $AP_S$ ,  $AP_M$ ,  $AP_L$  denote AP values for small, medium,

**Table 2**  
Comparison of Classification results on ImageNet-1K.

Model	Params (M)	GFLOPs	Accuracy (%)
PVTv2-b0 [33]	3.4	0.6	70.5
MobileNetV2×1.0 [26]	3.5	0.3	71.8
UniFormer-Tiny [11]	3.9	0.6	74.1
MSCViT-T [36]	3.8	0.5	73.9
DeiT-T [28]	5.7	1.3	72.2
MobileNetV3 0.75 [9]	4.0	0.2	73.3
EdgeViT-XXS [23]	4.1	0.6	74.4
CPVT-Ti-GAP [3]	6.0	1.3	74.9
SBCFormer-XS [19]	5.6	0.7	75.8
SDGFormer-T [34]	6.3	0.8	76.2
Mobile-Former-151M [2]	7.6	0.2	75.2
CaiT-xxs12-withDW[37]	6.6	1.3	75.89
Incepformer-S[22]	16.07	9.41	75.37
<b>SAEViT-T</b>	<b>6.0</b>	<b>0.8</b>	<b>76.3</b>
MobileNetV2×1.4 [26]	6.1	0.6	74.7
EdgeViT-XS [23]	6.7	1.1	77.5
MSCViT-XS [36]	7.7	1.0	77.3
PVT-T [32]	13.2	1.9	75.1
SBCFormer-X [19]	8.5	0.9	77.7
SDGFormer-S [34]	9.1	1.6	77.6
EfficientNet-B1 [27]	7.8	0.7	79.1
Mobile-Former-294M [2]	11.4	0.3	77.9
Mobile-Former-508M [2]	14.0	0.5	79.3
CaiT-xxs24-withDW[37]	12.0	2.5	79.66
Incepformer-M[22]	30.96	19.2	77.58
<b>SAEViT-XS</b>	<b>8.9</b>	<b>1.3</b>	<b>79.6</b>

**Table 3**  
Performance of SAEViT on RetinaNet.

Model	AP	$AP_{50}$	$AP_{75}$	$AP_S$	$AP_M$	$AP_L$
PoolFormer-S12[35]	36.2	56.2	38.2	20.8	39.1	48.0
PVTv2-B0[33]	37.2	57.2	39.5	23.1	40.4	49.7
EdgeViT-XXS[23]	38.7	59.0	41.0	22.4	42.0	51.6
SBCFormer-B[19]	39.3	59.8	41.5	21.9	<b>42.7</b>	<b>53.3</b>
<b>SAEViT-T</b>	<b>39.5</b>	<b>60.2</b>	<b>41.8</b>	<b>23.8</b>	42.5	53.1
PoolFormer-S24[35]	38.9	59.7	41.3	23.3	42.1	51.8
EdgeViT-XS[23]	40.6	61.3	43.3	25.2	43.9	54.6
SBCFormer-L[19]	41.1	62.3	43.3	24.7	44.3	<b>56.0</b>
<b>SAEViT-XS</b>	<b>41.8</b>	<b>62.5</b>	<b>44.5</b>	<b>25.6</b>	<b>44.9</b>	55.8

and large objects, respectively. For Mask R-CNN, box mAP and mask mAP are used as the primary evaluation metrics.

**Results:** The experimental results on the COCO dataset are detailed in Tables 3 and 4 by using RetinaNet and Mask R-CNN respectively. Apparently, SAEViT ranks first in each group. Especially, SAEViT-T and SAEViT-XS achieve 39.5 AP and 41.8 AP respectively, surpassing other competitors with safe margins. Similarly, using Mask R-CNN detector, SAEViT-T and SAEViT-XS achieve 40.1 AP and 42.6 AP respectively, which exhibits strong object localization and segmentation ability under complex scenes.

**Table 4**  
Performance of SAEViT on Mask R-CNN.

Model	$AP_b$	$AP_{50}^b$	$AP_{75}^b$	$AP^m$	$AP_{50}^m$	$AP_{75}^m$
EfficientFormer-L1[13]	37.9	60.3	41.0	35.4	57.3	37.3
<b>SAEViT-T</b>	<b>40.1</b>	<b>61.8</b>	<b>43.2</b>	<b>37.6</b>	<b>59.5</b>	<b>40.1</b>
RepViT-M1.1[30]	39.8	61.9	43.5	37.2	58.8	40.1
EfficientFormer-L3[13]	41.4	63.9	44.7	38.1	61.0	40.4
<b>SAEViT-XS</b>	<b>42.6</b>	<b>64.3</b>	<b>46.2</b>	<b>40.3</b>	<b>62.8</b>	<b>43.5</b>

**Table 5**  
Segmentation Results on ADE20K.

Model	Params(M)	mIoU
PVTv2-b0[33]	7.6	37.2
PoolFormer-S12[35]	7.6	37.2
EdgeViT-XXS[23]	7.9	39.7
<b>SAEViT-T</b>	<b>10.1</b>	<b>40.6</b>
RepViT-m1.1[30]	12.0	40.6
EdgeViT-XS[23]	10.6	41.4
PVT-S[32]	28.2	39.8
PoolFormer-S12[35]	23.2	40.3
EfficientFormer-L1[13]	12.3	38.9
<b>SAEViT-XS</b>	<b>13.1</b>	<b>42.1</b>

**Visualizations:** Fig. 4 shows detection results by using different detectors. The 1<sup>st</sup> and the 3<sup>rd</sup> columns shows the results of SAEViT-XS by using RetinaNet, the 2<sup>nd</sup> and the 4<sup>th</sup> columns show the results by using Mask R-CNN. Generally, they have all achieved detection tasks for commonly known objects, except that RetinaNet has some missed detections, while Mask R-CNN made some duplicated detections.

### 4.3. Semantic Segmentation on ADE20K

The semantic segmentation experiment is conducted on the ADE20K scene parsing dataset. The overall performance is evaluated using Semantic FPN detector. During training, the network is initialized with ImageNet pre-trained weights, and any newly added layers are initialized via Xavier initialization. The AdamW optimizer is used with an initial learning rate of  $1 \times 10^{-4}$ . Following common practice, our model is trained 80K epochs on a single NVidia 3090 GPU with a batch size of 16. The learning rate is adjusted using a polynomial decay schedule. During training, input images are randomly resized and cropped to 512×512. During testing, the image's shorter side is resized to 512 pixels. The evaluation metric is mIoU (i.e. mean Intersection over Union).

**Results:** On the ADE20K dataset, the results of SAEViT in semantic segmentation tasks are presented in Table 5. SAEViT-T achieves 40.6 mIoU, showing improved segmentation accuracy across different semantic categories and demonstrating precise recognition and segmentation of various objects and scenes within images. Meanwhile, SAEViT-XS obtains 42.1 mIoU, ensuring both accuracy and integrity in semantic segmentation under complex scenes.



Fig. 4: The detection results on COCO dataset.

#### 4.4. GPU Throughput and Latency tests

As the key indicator for measuring the real-time inference performance of deep learning models, while device latency directly reflects the response speed of the model in practical application scenarios such as real-time image recognition and autonomous driving decision systems. In this section, throughput and latency tests are implemented multiple times to measure the model’s average throughput (i.e. the number of images processed per second) and single-image inference latency (milliseconds) on a given device. The experimental setup includes a 5s warm-up period, random initialization of  $224 \times 224$  feature maps, and batch sizes set to 256 for throughput measurement and 1 for latency measurement; to ensure fairness and reduce error, forward propagation is run 50 times and the delay averaged. All tests are conducted on the same AMD Ryzen 7 5800H CPU and NVIDIA RTX 3060 Laptop GPU, comparing PVT-T, ShuntedViT-T, CMT-Ti and our model SAEViT-XS.

The results are shown in Table 6. Our model has the minimum number of parameters and relatively low computation cost. However, we achieve slightly lower accuracy than ShuntedViT-T, we realize the highest throughput and lowest latency among all the methods by safe margins.

#### 4.5. Ablation Studies

In this section, we will investigate the effectiveness of the core components of our model, as well as the advantages of SAA and CIFFN.

##### 4.5.1. Analysis of the core components in our model

In this section, we investigate the impacts of the core components, including SAA, CIFFN and LFE. Table 7 shows the classification accuracies by using and without using the 3 components. Specifically, SRA and FFN substitute SAA and CIFFN respectively. As mentioned earlier, LFE is an embedding layer with DWConv, which achieves smooth noise suppression and refines the input features to the Transformer block. It introduces only 0.1 M parameters and 0.01G computation, but brings 0.6% Top-1 accuracy improvement. Compared with SRA, SAA achieves 0.5% higher accuracy, the reason is that the deconvolution operation in SAA recovers more feature information than the spatial reduction in SRA. The common goal of SAA and SRA is to reduce the computational cost of self-attention through spatial downsampling. SRA only performs pooling or linear mapping on key and value tensors. By contrast, SAA processes the entire feature map by performing pooling on the normalized input and fusing it with the original features through skip connections. After attention operation,

**Table 6**

The comparison of throughputs and device Latency among several popular methods.

Model	Params(M)	GFLOPs	Throughput	Accuracy(%)	Latency(ms)
PVT-T[32]	13.2	1.9	420.55	75.1	44.62
ShuntedViT-T [25]	11.5	2.1	168.40	<b>79.8</b>	52.57
CMT-Ti[6]	9.5	<b>0.6</b>	496.36	79.1	60.88
<b>SAEViT-XS</b>	<b>8.9</b>	1.3	<b>575.89</b>	79.6	<b>36.80</b>

**Table 7**

Ablation experiment on the core components.

LFE	SAA	CIFFN	Accuracy(%)
			77.2
✓			77.8
✓	✓		78.3
✓	✓	✓	<b>79.6</b>

SAA uses deconvolution for upsampling to restore spatial resolution, which is different from SRA. After  $s_r \times s_r$  spatial down-sampling, it reconstructs the spatial structure through deconvolution to preserve high-frequency edges and textures. Although it introduces 0.3M parameters and 0.02G computation, it also improves Top-1 accuracies. CIFFN makes the greatest increase in accuracy than LFE and SAA, as its channel-wise feature selection and integration facilitate more effective feature learning. CIFFN uses channel decomposition and learnable channel-level re-calibration to filter and redistribute channel-level information. It yields 79.6% accuracy at the cost of 0.4M parameters and 0.03G computation. It's worth noting that the 3 modules introduces less than 1M parameters, but improves the accuracy by 2.4%, which strikes a balance between lightweight design and performance gain.

#### 4.5.2. Computational Efficiency of Attention Modules

In this section, we compare the comprehensive performances of different attention modules in terms of number of parameters, computation cost, the throughput of both CPU and GPU, so as to investigate the computational efficiency of different attention modules. Specifically, the processing speed of the attention modules is tested on both an AMD Ryzen 7 5800H CPU and an NVIDIA RTX 3060 Laptop GPU. All attention modules adopt identical settings: the input dimension is  $X \in X^{H \times W \times C}$ , where  $H=W=56$ , and  $C=256$ . The multi-head attention mechanism has 8 heads, and the input batch size is 128. All other conditions remain identical. As shown in Table 8, SAA has the lowest computation cost and almost the lowest number of parameters, but it realizes the highest CPU and GPU throughputs (i.e. it processes 8187 images/sec on AMD Ryzen 7 5800H and 22942 images/sec on NVidia RTX 3060). This results demonstrate that our SAA has obvious advantage in processing efficiency, especially SAA is more CPU-friendly than other methods.

**Table 8**

Comprehensive performance comparison among our proposed SAA and other popular attention modules.

Attention Modules	Params(M)	FLOPs	CPU	GPU
SRA[32]	0.53	1979.14	2674	17345
Cross Attention[5]	0.27	1458.72	5002	18706
Shifted Window[18]	0.26	900.76	6058	13479
HIRO[24]	<b>0.25</b>	1609.65	3342	20772
MSC[36]	0.41	2422.35	2131	11123
SAA	0.26	<b>679.18</b>	<b>8187</b>	<b>22942</b>

#### 4.5.3. Inter-channel Enhancement Effect of CIFFN

In this section, the channel correlation results among FFN, DWFFN and CIFFN will be investigated, exploring the inter-channel enhancement effect of CIFFN. To be specific, 3 models with FFN/DWFFN/CIFFN respectively are pre-trained on Tiny ImageNet. Tiny ImageNet, a sub-set of ImageNet, is a challenging benchmark for image classification. It has 200 different categories, each of which has 500 images for training, 50 for validation and 50 for testing. In this test, the intermediate features of the 3rd stage of our model (as shown in Fig. 1) are captured in the forward propagation process to analyze the channel correlation. We randomly select 100 channels for correlation analysis through down-sampling, where we calculate the correlation matrices between different channels, and generate heatmaps and corresponding statistical information. This experiment is carried out on a laptop with AMD Ryzen 7 5800H processor and NVIDIA RTX 3060. As shown in Fig. 5, the horizontal axis of the histogram shows the correlation between different channels (ranging from -1 to 1, the larger the abs mean, the more relevant they are, 0 denotes irrelevant). The vertical axis shows the number of relevant channels in each interval (i.e. frequency). Furthermore, Fig. 6 displays the heatmaps of inter-channel correlations produced by FFN, DWFFN and CIFFN respectively (both horizontal and vertical axis are selected channels). Red/Orange colors indicate higher relevance, while blue indicates less relevant, white denotes irrelevant. Based on Fig. X apparently CIFFN has lower Abs Mean and Standard deviation (Std), indicating that CIFFN has lower channel redundancy than FFN. As shown in Fig. 6, the overall response of FFN exhibits warm colors in certain areas, reflecting the high correlation and redundancy between its channels. DWFFN, on the other hand, exhibits weak correlations by its evenly distributed cold colors, indicating strong independence among its channels (i.e. a lack of interaction). By contrast, CIFFN makes warmer

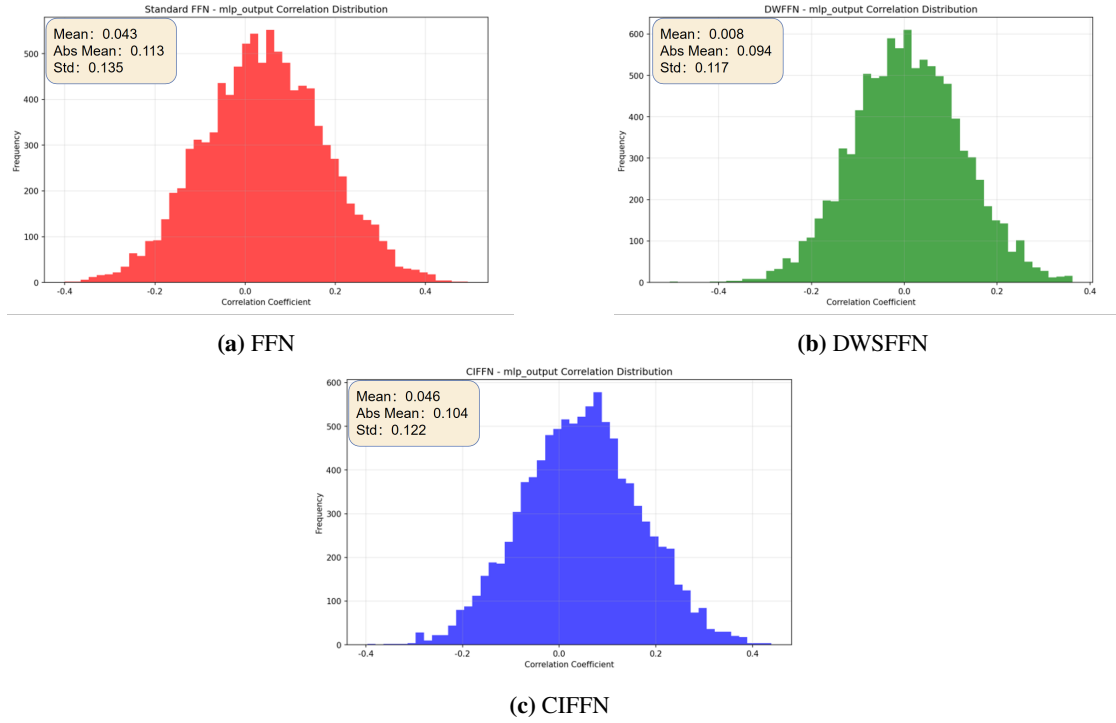


Fig. 5: Comparison of correlation coefficient among FFN, DWFFN and CIFFN.

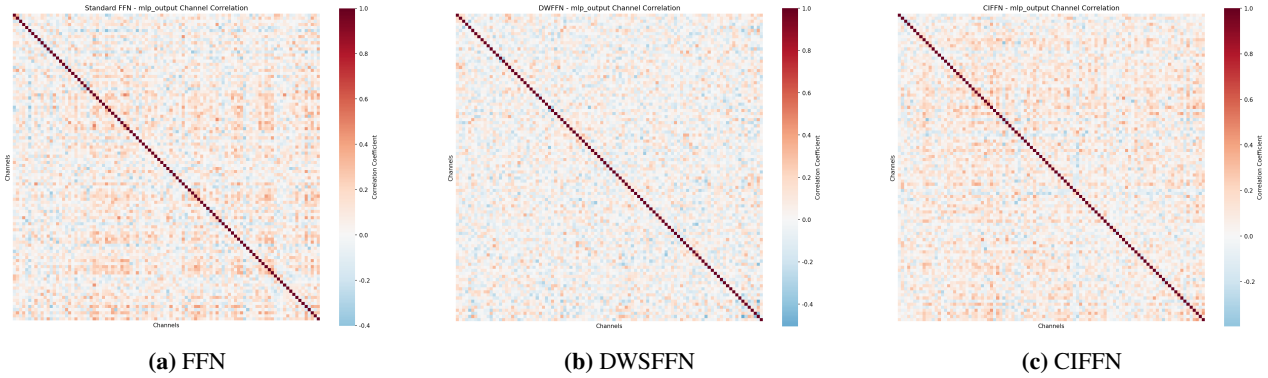


Fig. 6: Comparison of Channel correlation heatmap.

colors than DWFFN, which are more evenly distributed than FFN. This phenomenon illustrates that CIFFN maintains highly correlated channel groups and necessary feature diversity while reducing the overall redundancy.

#### 4.5.4. The role of the conv-stem

The conv-stem plays a critical role in ViT families. We propose to employ a conv-stem head (instead of using a patch embedding) for down-sampling. When the input feature map is  $224 \times 224$ , the patch size is set to 4 in the initial stage. After the first down-sampling layer, the image dimension is reduced to 1/4 of the original size (i.e.  $56 \times 56$ ). However, it may cause the loss of more fine-grained features. An experiment has been conducted on ImageNet-1K to testify the function of

Table 9

The influence of conv-stem on SAEViT-T.

Model Architecture	Params(M)	Accuracy(%)
Without conv-stem	5.98	74.89
Using conv-stem	6.04	<b>76.28</b>

conv-stem on accuracy. As shown in Table 9, using conv-stem brings obvious higher accuracy without substantially increasing computational costs.

## 5. Conclusion

In this paper, we propose SAEViT, a hybrid ViT based architecture for various vision tasks. The core components include Sparsely Aggregated Attention and channel-interactive Feed-Forward Network. By fusing the local prior capability of the convolution blocks with ViT's global modeling strengths, SAEViT significantly enhances the performances while maintaining relatively low computational overhead. Extensive experiments have been conducted on 3 different vision tasks to validate its effectiveness, where the advantage in the accuracy-speed tradeoff has been highlighted against other methods. Additional ablation experiments are also carried out to verify the function of the core components. Although effective, SAEViT has some limitations under special scenarios. Firstly, the SAA module performs global static downsampling based on token redundancy, but for areas with rich details or small targets, it may cause excessive compressed information and therefore results in lower recognition accuracy for fine-grained features. Meanwhile, its fixed sampling rate also limits its adaptability to high-resolution inputs. Secondly, although CIFFN enhances inter-channel feature interaction, it still induces certain computational and memory overhead due to the depth-wise separable convolution and re-assignment operations, which may affect deployment efficiency in resource constrained environments. In the future, we will focus on developing dynamic or layered sparse sampling methods to preserve key information, and introducing learnable multi-scale attention mechanisms to enhance adaptability to different input resolutions. And in the future, we will develop more efficient sparse sampling strategies and deploy the model to edge devices to exert its role in practical situations.

## References

- [1] Cai, H., Li, J., Hu, M., Gan, C., Han, S., 2023. Efficientvit: Lightweight multi-scale attention for high-resolution dense prediction, in: Proceedings of the IEEE/CVF international conference on computer vision, pp. 17302–17313.
- [2] Chen, Y., Dai, X., Chen, D., Liu, M., Dong, X., Yuan, L., Liu, Z., 2022. Mobile-former: Bridging mobilenet and transformer, in: Proceedings of the IEEE/CVF Conference on Computer Vision and Pattern Recognition (CVPR), pp. 5270–5279.
- [3] Chu, X., Tian, Z., Zhang, B., Wang, X., Shen, C., 2023. Conditional positional encodings for vision transformers, in: The Eleventh International Conference on Learning Representations. URL: <https://openreview.net/forum?id=3KWnuT-R1bh>.
- [4] Deng, J., Dong, W., Socher, R., Li, L.J., Li, K., Fei-Fei, L., 2009. Imagenet: A large-scale hierarchical image database, in: 2009 IEEE conference on computer vision and pattern recognition, Ieee. pp. 248–255.
- [5] Dong, X., Bao, J., Chen, D., Zhang, W., Yu, N., Yuan, L., Chen, D., Guo, B., 2022. Cswin transformer: A general vision transformer backbone with cross-shaped windows, in: Proceedings of the IEEE/CVF conference on computer vision and pattern recognition, pp. 12124–12134.
- [6] Guo, J., Han, K., Wu, H., Tang, Y., Chen, X., Wang, Y., Xu, C., 2022. Cmt: Convolutional neural networks meet vision transformers, in: Proceedings of the IEEE/CVF conference on computer vision and pattern recognition, pp. 12175–12185.
- [7] Hatamizadeh, A., Heinrich, G., Yin, H., Tao, A., Alvarez, J.M., Kautz, J., Molchanov, P., . Fastervit: Fast vision transformers with hierarchical attention, in: The Twelfth International Conference on Learning Representations.
- [8] He, K., Gkioxari, G., Dollár, P., Girshick, R., 2017. Mask r-cnn, in: Proceedings of the IEEE international conference on computer vision, pp. 2961–2969.
- [9] Howard, A., Sandler, M., Chu, G., Chen, L.C., Chen, B., Tan, M., Wang, W., Zhu, Y., Pang, R., Vasudevan, V., et al., 2019. Searching for mobilenetv3, in: Proceedings of the IEEE/CVF international conference on computer vision, pp. 1314–1324.
- [10] Huang, T., Huang, L., You, S., Wang, F., Qian, C., Xu, C., 2022. Lightvit: Towards light-weight convolution-free vision transformers. arXiv preprint arXiv:2207.05557 .
- [11] Li, K., Wang, Y., Peng, G., Song, G., Liu, Y., Li, H., Qiao, Y., 2022a. Unifomer: Unified transformer for efficient spatial-temporal representation learning, in: International Conference on Learning Representations. URL: [https://openreview.net/forum?id=nBU\\_u6DLvoK](https://openreview.net/forum?id=nBU_u6DLvoK).
- [12] Li, S., Liu, N., Li, Y., Zhang, Y., 2023. Qpdet: A queuing people detector for aerial images. IEEE Geoscience and Remote Sensing Letters 20, 1–5. doi:10.1109/LGRS.2023.3294271.
- [13] Li, Y., Yuan, G., Wen, Y., Hu, J., Evangelidis, G., Tulyakov, S., Wang, Y., Ren, J., 2022b. Efficientformer: Vision transformers at mobilenet speed. Advances in Neural Information Processing Systems 35, 12934–12949.
- [14] Liang, J., Cui, Y., Wang, Q., Geng, T., Wang, W., Liu, D., 2023a. Clusterfomer: Clustering as a universal visual learner, in: Oh, A., Naumann, T., Globerson, A., Saenko, K., Hardt, M., Levine, S. (Eds.), Advances in Neural Information Processing Systems, Curran Associates, Inc.. pp. 64029–64042. URL: [https://proceedings.neurips.cc/paper\\_files/paper/2023/file/c9ef471a579197c4ed99df2aa542ce97-Paper-Conference.pdf](https://proceedings.neurips.cc/paper_files/paper/2023/file/c9ef471a579197c4ed99df2aa542ce97-Paper-Conference.pdf).
- [15] Liang, J.C., Zhou, T., Liu, D., Wang, W., 2023b. CLUSTSEG: Clustering for universal segmentation, in: Krause, A., Brunskill, E., Cho, K., Engelhardt, B., Sabato, S., Scarlett, J. (Eds.), Proceedings of the 40th International Conference on Machine Learning, PMLR. pp. 20787–20809. URL: <https://proceedings.mlr.press/v202/liang23h.html>.
- [16] Lin, T.Y., Goyal, P., Girshick, R., He, K., Dollár, P., 2017. Focal loss for dense object detection, in: Proceedings of the IEEE international conference on computer vision, pp. 2980–2988.
- [17] Lin, T.Y., Maire, M., Belongie, S., Hays, J., Perona, P., Ramanan, D., Dollár, P., Zitnick, C.L., 2014. Microsoft coco: Common objects in context, in: Computer vision—ECCV 2014: 13th European conference, zurich, Switzerland, September 6–12, 2014, proceedings, part v 13, Springer. pp. 740–755.
- [18] Liu, Z., Lin, Y., Cao, Y., Hu, H., Wei, Y., Zhang, Z., Lin, S., Guo, B., 2021. Swin transformer: Hierarchical vision transformer using shifted windows, in: Proceedings of the IEEE/CVF international conference on computer vision, pp. 10012–10022.
- [19] Lu, X., Sukanuma, M., Okatani, T., 2024a. Sbcformer: lightweight network capable of full-size imagenet classification at 1 fps on single board computers, in: Proceedings of the IEEE/CVF Winter Conference on Applications of Computer Vision, pp. 1123–1133.
- [20] Lu, Y., Liu, D., Wang, Q., Han, C., Cui, Y., Cao, Z., Zhang, X., Chen, Y.V., Fan, H., 2024b. Promotion: Prototypes as motion learners, in: 2024 IEEE/CVF Conference on Computer Vision and Pattern Recognition (CVPR), pp. 28109–28119. doi:10.1109/CVPR52733.2024.02655.
- [21] Mehta, S., Rastegari, M., 2022. Mobilevit: Light-weight, general-purpose, and mobile-friendly vision transformer, in: International Conference on Learning Representations. URL: <https://openreview.net/forum?id=vh-0sUt8HlG>.
- [22] Meng, W., Huang, Z., Liu, Q., Cai, M., Chen, K., Ma, L., 2025. Spike-driven inceptionformer: A hierarchical spiking transformer with inception-inspired feature learning. Neurocomputing 648, 130727. URL: <http://www.sciencedirect.com/science/article/pii/S0925231225013992>.

- doi:<https://doi.org/10.1016/j.neucom.2025.130727>.
- [23] Pan, J., Bulat, A., Tan, F., Zhu, X., Dudziak, L., Li, H., Tzimiropoulos, G., Martinez, B., 2022a. Edgevits: Competing light-weight cnns on mobile devices with vision transformers, in: European conference on computer vision, Springer. pp. 294–311.
- [24] Pan, Z., Cai, J., Zhuang, B., 2022b. Fast vision transformers with hilo attention. *Advances in Neural Information Processing Systems* 35, 14541–14554.
- [25] Ren, S., Zhou, D., He, S., Feng, J., Wang, X., 2022. Shunted self-attention via multi-scale token aggregation, in: Proceedings of the IEEE/CVF conference on computer vision and pattern recognition, pp. 10853–10862.
- [26] Sandler, M., Howard, A., Zhu, M., Zhmoginov, A., Chen, L.C., 2018. Mobilenetv2: Inverted residuals and linear bottlenecks, in: Proceedings of the IEEE conference on computer vision and pattern recognition, pp. 4510–4520.
- [27] Tan, M., Le, Q., 2019. Efficientnet: Rethinking model scaling for convolutional neural networks, in: International conference on machine learning, PMLR. pp. 6105–6114.
- [28] Touvron, H., Cord, M., Douze, M., Massa, F., Sablayrolles, A., Jégou, H., 2021. Training data-efficient image transformers & distillation through attention, in: International conference on machine learning, PMLR. pp. 10347–10357.
- [29] Tu, Z., Talebi, H., Zhang, H., Yang, F., Milanfar, P., Bovik, A., Li, Y., 2022. Maxvit: Multi-axis vision transformer, in: European conference on computer vision, Springer. pp. 459–479.
- [30] Wang, A., Chen, H., Lin, Z., Han, J., Ding, G., 2024. Repvit: Revisiting mobile cnn from vit perspective, in: Proceedings of the IEEE/CVF Conference on Computer Vision and Pattern Recognition, pp. 15909–15920.
- [31] Wang, W., Han, C., Zhou, T., Liu, D., 2023. Visual recognition with deep nearest centroids, in: The Eleventh International Conference on Learning Representations. URL: <https://openreview.net/forum?id=CsKwajvr7A>.
- [32] Wang, W., Xie, E., Li, X., Fan, D.P., Song, K., Liang, D., Lu, T., Luo, P., Shao, L., 2021. Pyramid vision transformer: A versatile backbone for dense prediction without convolutions, in: Proceedings of the IEEE/CVF international conference on computer vision, pp. 568–578.
- [33] Wang, W., Xie, E., Li, X., Fan, D.P., Song, K., Liang, D., Lu, T., Luo, P., Shao, L., 2022. Pvt v2: Improved baselines with pyramid vision transformer. *Computational visual media* 8, 415–424.
- [34] Wen, C., Gong, X., 2023. Sdgformer: An efficient convolution network structurally similar to transformer, in: 2023 IEEE International Conference on Multimedia and Expo (ICME), IEEE. pp. 1181–1186.
- [35] Yu, W., Luo, M., Zhou, P., Si, C., Zhou, Y., Wang, X., Feng, J., Yan, S., 2022. Metaformer is actually what you need for vision, in: Proceedings of the IEEE/CVF conference on computer vision and pattern recognition, pp. 10819–10829.
- [36] Zhang, B., Zhang, Y., 2025. Mscvit: A small-size vit architecture with multi-scale self-attention mechanism for tiny datasets. *Neural Networks* 188, 107499.
- [37] Zhang, T., Xu, W., Luo, B., Wang, G., 2025. Depth-wise convolutions in vision transformers for efficient training on small datasets. *Neurocomputing* 617, 128998. URL: <https://www.sciencedirect.com/science/article/pii/S0925231224017697>, doi:<https://doi.org/10.1016/j.neucom.2024.128998>.
- [38] Zhang, Z., Zhang, H., Zhao, L., Chen, T., Arik, S.Ö., Pfister, T., 2022. Nested hierarchical transformer: Towards accurate, data-efficient and interpretable visual understanding, in: Proceedings of the AAAI Conference on Artificial Intelligence, pp. 3417–3425.
- [39] Zhou, B., Zhao, H., Puig, X., Fidler, S., Barriuso, A., Torralba, A., 2017. Scene parsing through ade20k dataset, in: Proceedings of the IEEE conference on computer vision and pattern recognition, pp. 633–641.
- [40] Zhou, Y., Li, Z., Guo, C.L., Bai, S., Cheng, M.M., Hou, Q., 2023. Srformer: Permuted self-attention for single image super-resolution, in: Proceedings of the IEEE/CVF International Conference on Computer Vision, pp. 12780–12791.
- [41] Zhu, L., Wang, X., Ke, Z., Zhang, W., Lau, R.W., 2023. Biformer: Vision transformer with bi-level routing attention, in: Proceedings of the IEEE/CVF conference on computer vision and pattern recognition, pp. 10323–10333.